2.1 Å Crystal Structure of Human PXR in Complex with the St. John's Wort Compound Hyperforin[†,‡]

Ryan E. Watkins,[§] Jodi M. Maglich,[∥] Linda B. Moore,[∥] G. Bruce Wisely,[∥] Schroeder M. Noble,[§] Paula R. Davis-Searles,[§] Mill H. Lambert,[∥] Steven A. Kliewer,[∥,⊥] and Matthew R. Redinbo*[,§]

Departments of Chemistry and Biochemistry & Biophysics and the Lineberger Comprehensive Cancer Center, The University of North Carolina at Chapel Hill, North Carolina 27599, and Nuclear Receptor Discovery Research, GlaxoSmithKline, Research Triangle Park, North Carolina 27709

Received September 20, 2002; Revised Manuscript Received November 21, 2002

ABSTRACT: The nuclear xenobiotic receptor PXR is activated by a wide variety of clinically used drugs and serves as a master regulator of drug metabolism and excretion gene expression in mammals. St. John's wort is used widely in Europe and the United States to treat depression. This unregulated herbal remedy leads to dangerous drug−drug interactions, however, in patients taking oral contraceptives, antivirals, or immunosuppressants. Such interactions are caused by the activation of the human PXR by hyperforin, the psychoactive agent in St. John's wort. In this study, we show that hyperforin induces the expression of numerous drug metabolism and excretion genes in primary human hepatocytes. We present the 2.1 Å crystal structure of hyperforin in complex with the ligand binding domain of human PXR. Hyperforin induces conformational changes in PXR's ligand binding pocket relative to structures of human PXR elucidated previously and increases the size of the pocket by 250 Å^3. We find that the mutation of individual aromatic residues within the ligand binding cavity changes PXR's response to particular ligands. Taken together, these results demonstrate that PXR employs structural flexibility to expand the chemical space it samples and that the mutation of specific residues within the ligand binding pocket of PXR tunes the receptor's response to ligands.

Cytochrome P450 (CYP)[1] enzymes, conjugating enzymes, and transporters play an important role in protecting organisms against both endogenous (endobiotics) and exogenous (xenobiotics) toxic chemicals. Exposure to xenobiotics can result in the induction of genes encoding these chemoprotective proteins. This adaptive response provides a mechanism for protecting the organism during periods of chemical stress.

The pregnane X receptor (PXR; NR1I2) serves as a key regulator of the adaptive response to xenobiotics in mammals (*1*, *2*). PXR is a member of the nuclear receptor family of ligand-activated transcription factors that includes receptors for the steroid, retinoid, and thyroid hormones. Unlike the classical nuclear hormone receptors, which are specific for their cognate hormones, PXR is activated by a structurally diverse collection of compounds. Upon activation, PXR binds to DNA and regulates a large program of genes in the liver and intestine that are involved in the metabolism and excretion of potentially harmful xenobiotics including those encoding CYPs, glutathione-S-transferases, UDP-glucuronosyltransferases, sulfotransferases, and transporters (*1*).

Although PXR evolved to protect the body, it is also responsible for an important class of harmful drug−drug interactions. PXR is activated by many prescription drugs including the antibiotic rifampicin, the antihypertensive drugs nifedipine and spironolactone, and the cancer drug paclitaxel (*3*−*6*). Activation of PXR can accelerate the metabolism of other drugs taken concurrently, thereby reducing their clinical efficacy. Recently, two groups demonstrated that PXR is potently activated by hyperforin (Figure 1), the psychoactive constituent of the widely used herbal antidepressant St. John's wort (SJW) (*7*, *8*). This finding provided a molecular explanation for the clinical observation that SJW can accelerate the metabolism of a wide variety of prescription drugs including immunosuppressants, HIV protease inhibitors, and cancer drugs, sometimes with life-threatening consequences (*9*−*14*).

We recently described the crystal structure of the PXR ligand binding domain (LBD) in both the apo state and bound

[†] This study was supported by research grants from the National Institutes of Health (DK62229, CA77340), a Burroughs Wellcome Career Award in the Biomedical Sciences, and a Glaxo−UNC Collaborative Grant (M.R.R.).

[‡] Atomic coordinates have been deposited with the RCSB (PDB ID: 1M13).

* To whom correspondence should be addressed. Phone: (919) 843-8910. Fax: (919) 966-3675. E-mail: redinbo@unc.edu.

[§] The University of North Carolina at Chapel Hill.

[∥] GlaxoSmithKline.

[⊥] Present address: Department of Molecular Biology, UT Southwestern Medical Center, Building NC7.214E, 5323 Harry Hines Blvd., Dallas, TX 75390-8594.

[1] Abbreviations: PXR, pregnane X receptor; CYP, cytochrome P450; NR, nuclear receptor; LBD, ligand binding domain; UDP, uridine diphosphate; SJW, Saint John's wort; HIV, human immunodeficiency virus; SR12813, 3,5-di-*tert*-butyl-4-hydroxystyrene-β,β-diphosphonic acid tetraethyl ester; SRC-1, steroid receptor coactivator-1; rmsd, root-mean-square deviation; AF, activation function; PPAR, peroxisome proliferator-activated receptor; EC_{50}, median effective concentration; CV-1, African green monkey kidney fibroblasts; PCR, polymerase chain reaction.

10.1021/bi0268753 CCC: $25.00
Published on Web 01/24/2003

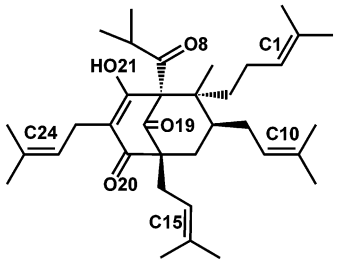

FIGURE 1: Chemical structure of hyperforin.

to the cholesterol-lowering drug SR12813 (*15*). PXR has several unique characteristics that account for its promiscuous ligand binding properties, including a large elliptical ligand binding pocket that allows SR12813 to bind in three distinct orientations. In this report, we describe the crystal structure of the PXR LBD bound to hyperforin and demonstrate that the ligand binding pocket can be induced to adopt different shapes depending upon which ligand is bound. We propose that this induced fit model is critical for the promiscuous ligand binding properties of PXR.

MATERIALS AND METHODS

Gene Expression Studies Using Real-Time Quantitative PCR. Human hepatocytes were purchased from BioWhittaker, Inc. (Walkersville, MD). Tissues were maintained in Williams' Medium E (Invitrogen) supplemented with 100 nM dexamethasone (Invitrogen; Rockville, MD), L-glutamine 2 mM (Invitrogen), and insulin−transferrin−selenium (ITS, Invitrogen) and were treated with either rifampicin (10 μM) or hyperforin (0.6 μM). Control cultures received DMSO alone. Cells were treated at 0 and 24 h and harvested at 48 h. Total RNA was isolated using the TRIzol reagent (Invitrogen) according to the manufacturer's instructions. Real-time quantitative PCR (RTQ-PCR) was performed using an ABI PRISM 7700 Sequence Detection System instrument and software (PE Applied Biosystems, Inc., Foster City, CA). RNA samples were diluted to 100 μg/mL and treated with 40 U/mL RNAse-free deoxyribonuclease I for 30 min at 37 °C followed by inactivation at 75 °C for 5 min. Samples were quantified by spectrophotometry, diluted to 10 ng/μL, and then assayed in duplicate 25 μL reactions using 25 ng of RNA/reaction. Gene-specific primers were used at 7.5 or 23 pmol/reaction, and gene-specific probes were used at 5 pmol/reaction. Primers and probes were designed using Primer Express Version 2.0.0 (Applied Biosystems), synthesized by Keystone Laboratories (Camarillo, CA), and validated by NCBI Blast. Fold induction values were calculated by subtracting the mean threshold cycle number (Ct) for each treatment group from the mean Ct for the vehicle group and raising 2 to the power of this difference (Table 1).

Crystallization and Structure Determination. The hPXR−LBD (comprising residues 130−434) was coexpressed with an SRC-1 fragment (residues 623−710) in *Escherichia coli* and purified as described (*15*). The SRC-1 fragment remains with the PXR−LBD after purification by SDS−PAGE analysis but does not join the crystals of PXR (*15*). hPXR−LBD was concentrated to 5 mg/mL in buffer containing 20 mM Tris-HCl (pH 7.80), 250 mM NaCl, 5% glycerol (v/v), 5 mM DTT, 2.5 mM EDTA, and a 2-fold molar excess of hyperforin (Apin Chemicals Limited) using centriprep YM-30's (Amicon). The PXR−hyperforin complex was crystallized using hanging drop vapor diffusion at 22 °C against buffer containing 50 mM imidazole (pH 7.6) and 12% 2-propanol, and crystals were handled as described (*15*). Data were collected using a Rigaku RUH3R generator with Osmic Confocal Blue Optics and an R-Axis IV++ detector and processed using DENZO/SCALEPACK (*16*) (Table 2). The structure was determined by molecular replacement with AMoRe (*17*) using the structure of apo PXR (*15*) as the search model. Structure refinement involved O (*18*), torsion angle refinement in CNS (*19*) with the maximum likelihood function target, and $2|F_{obs}| - |F_{calc}|$, $|F_{obs}| - |F_{calc}|$ and composite-annealed omit electron density maps. Residues 142−177 and 198−434 are present in the final model, including three novel residues (432−434) at the C-terminus. Unbiased electron density for hyperforin was obtained by calculating 2.5 Å $|F_{obs}| - |F_{obs}|$ density maps between the hyperforin and apo datasets; the R_{iso} value between these

Table 1: Regulation of Gene Expression in Primary Human Hepatocytes[a]

gene	UniGene code	hyperforin (0.6 μM)	rifampicin (10 μM)
cytochrome P450 3A4	CYP3A4	26×	56×
cytochrome P450 2B6	CYP2B6	3.0×	2.8×
cytochrome P450 1A1	CYP1A1	15×	12×
cytochrome P450 1A2	CYP1A2	5.3×	7.7×
cytochrome P450 1B1	CYP1B1	1.7×	1.7×
cytochrome P450 2C8	CYP2C8	1.6×	2.9×
cytochrome P450 2C9	CYP2C9	1.9×	3.2×
P450 oxidoreductase	POR	1.8×	2.8×
multidrug resistance protein 1 (MDR1)	ABCB1	1.5×	1.5×
epoxide hydrolase	EPHX1	3.2×	6.2×
aldehyde dehydrogenase 1A1	ALDH1A1	2.0×	3.2×
glutathione S-transferase A2	GSTA2	3.2×	10×

[a] Fold change in mRNA levels relative to uninduced control samples.

Table 2: Crystallographic Statistics for the PXR−Hyperforin Complex Structure

resolution (Å; highest shell)	20−2.15 (2.23−2.15)
space group	$P4_32_12$
cell constants (Å)	$a = b = 91.4$; $c = 85.6$
reflections	
total	107 452
unique	20 273
mean redundancy	5.3
Wilson B-factor (Å^2)	21.4
R_{sym} (%)[a]	5.7 (37.7)
completeness (%)	99.4 (100)
mean I/σ	23.7 (4.7)
R_{cryst} (%)[b]	21.2 (23.5)
R_{free} (%)[c]	24.6 (27.8)
rms[d] deviation	
bond lengths (Å)	0.006
bond angles (deg)	1.1
dihedrals (deg)	21.0
impropers (deg)	0.75
number of atoms	
protein	2218
solvent	265
ligand	39

[a] $R_{sym} = \sum|I - \langle I\rangle|/\sum I$, where I is the observed intensity, and $\langle I\rangle$ is the average intensity of multiple symmetry-related observations of that reflection. [b] $R_{cryst} = \sum||F_{obs}| - |F_{calc}||/\sum|F_{obs}|$, where F_{obs} and F_{calc} are the observed and calculated structure factors, respectively. [c] $R_{free} = \sum||F_{obs}| - |F_{calc}||/\sum|F_{obs}|$ for 5% of the data not used at any stage of structural refinement. [d] rms: root-mean-square.

Table 3: EC_{50} Values (in nM) for Human PXR Variants in Response to Hyperforin, SR12813, and Rifampicin

ligand	wild type	F288A	W299M	H407Q
hyperforin	32.2 ± 7.7	13.4 ± 3.5	80.4 ± 17.6	56.7 ± 10.3
SR12813	127 ± 23.4	245 ± 35.6	78.0 ± 18.5	76.8 ± 15.8
rifampicin	463 ± 63.6	1,040 ± 107	748 ± 127	745 ± 154

data sets is 0.138 to 2.5 Å resolution. A total of 265 solvent sites were added late in refinement. The final model exhibits good geometry and no Ramachandran outliers. Figures were created using GRASP (*20*), MolScript (*21*), and DINO (*22*).

Cotransfection Assays with Mutant Forms of PXR. CV-1 cells were plated in 96-well plates at a density of 20 000 cells/well in phenol red-free Dulbecco's modified Eagle's medium containing high glucose and supplemented with 10% charcoal/dextran treated fetal bovine serum (HyClone, Logan, UT). Transfection mixes contained 5 ng of receptor expression vector, 20 ng of reporter plasmid, 12 ng of β-actin SPAP as internal control, and 43 ng of carrier plasmid. Wild type human PXR expression plasmid and the XREM−CYP3A4−LUC reporter, containing the enhancer and promoter of the CYP3A4 gene driving Luciferase expression, were as previously described (*3*, *23*). Single-site mutations of hPXR (F288A, W299M, and H407Q) were generated by PCR-based mutagenesis and were confirmed by DNA sequencing. Transfections were performed with LipofectAMINE (Life Technologies, Inc., Grand Island, NY) essentially according to the manufacturer's instructions. Drug dilutions were prepared in phenol red-free Dulbecco's modified Eagle's medium/F-12 medium with 15 mM HEPES supplemented with 10% charcoal-stripped, delipidated calf serum (Sigma, St. Louis, MO) that had previously been heat-inactivated at 62 °C for 35 min. Serial dilutions of hyperforin (Apin Chemical Co. Abingdon, Oxon, UK), SR 12813 (synthesized in-house), and rifampicin (Sigma, St. Louis, MO) were performed in triplicate to generate 11-point concentration response curves. Cells were incubated for 24 h in the presence of drugs, after which the medium was sampled and assayed for alkaline phosphatase activity. Luciferase reporter activity was measured using the LucLite assay system (Packard Instrument Co., Meriden, CT) and normalized to alkaline phosphatase activity (Table 3). EC_{50} values were determined by standard methods. None of these mutations impacted the basal activation level of the receptor relative to wild-type PXR (data not shown).

RESULTS

Gene Regulation by Hyperforin. The use of the unregulated herbal antidepressant St. John's wort in conjunction with other medications can cause a dangerous class of drug−drug interactions generated by the activation of PXR by hyperforin, an active agent in St. John's wort (*7*, *8*). St. John's wort has been shown to activate the expression, protein levels, and activity of P-glycoprotein and CYP3A in human cells (*24*, *25*), as well as CYP3A and CYP2E1 in mouse cells (*26*). To examine additional effects of hyperforin on human liver cells, we determined which genes were regulated by PXR in primary human hepatocytes treated with either hyperforin or rifampicin. Rifampicin was included as a control because it is an established activator of human PXR (*3*, *4*). We examined the changes in mRNA levels of 12 drug metabolism genes that were previously described as regulated by PXR (*6*, *27*, *28*). Genes examined included those involved in the oxidation (Phase I), conjugation (Phase II), and transport (Phase III) stages of drug metabolism and export (Table 1). Phase I drug metabolism genes up-regulated by hyperforin included aldehyde dehydrogenase 1A1 and seven cytochrome P450 (CYP) enzymes. CYP3A4 showed the largest fold induction by hyperforin (26×); CYP3A4 is the most abundant and promiscuous cytochrome P450 in human liver and metabolizes more than 50% of human drugs (*29*). CYP1A1, which processes several environmental carcinogens (*30*), also showed a high level of induction by hyperforin (15×). The CYP2C isoforms induced by hyperforin play a role in the metabolism of numerous therapeutic drugs including tolbutamin, warfarin, and taxol (*31*, *32*). The expression of P450 oxidoreductase, which is required for the synthesis of heme molecules for P450 enzymes, was also up-regulated by hyperforin. Expression of the Phase II glutathione S-transferase A2 allele and the Phase III efflux pump MDR1 were up-regulated 3.2- and 1.5-fold, respectively, by hyperforin. Thus, hyperforin induces the expression of a wide array of drug metabolism genes in human liver. The increased expression of these drug metabolism and excretion proteins is likely to explain the drug−drug interactions caused by St. John's wort.

Structure of the Hyperforin−PXR Complex. We next determined the crystal structure of the human PXR LBD in complex with hyperforin to 2.15 Å resolution (Figure 2A, Table 2). The hPXR−LBD, like other nuclear receptor ligand binding domains, is composed of a seven member α-helical sandwich arranged in three layers: α1/α3, α4/α5/α8, and α7/α10. While human PXR contains the canonical ligand binding domain fold in the α-helical portion of the receptor, it deviates from all known nuclear receptors in its extended, five-stranded antiparallel β sheet (*15*, *33*). This five-stranded β sheet forms a wall that frames one side of the large ligand binding cavity of PXR (Figure 2A). Nuclear receptor ligand binding domains typically contain three-stranded antiparallel β sheets. The PXR sequence that creates this extended β sheet shares little sequence identity with other nuclear receptors and appears to be a novel insert within PXR. A region of this sequence, residues 178−197, is unstructured in all the PXR ligand binding domain structures determined to date (*15*).

The PXR−hyperforin complex is similar to the structures of unliganded (apo) and SR12813-bound PXRs determined previously (*15*), with root-mean-square deviation (rmsd) values of 1.1 and 1.2 Å over all atoms, respectively. The α helix containing the ligand-dependent activation function (αAF) of hPXR−LBD, like the apo and SR12813 structures, is in an active orientation and appears permissive to binding coactivators. Despite this overall similarity, the PXR−hyperforin complex exhibits novel structural features. A pseudo-helical region comprising residues 198−210 begins the ordered portion of the structure after the 20-residue disordered region from amino acids 178−199. This pseudo-helical region shifts by 4.2 Å relative to the apo and SR12813-bound structures of PXR (*15*). In addition, a mobile hydrophobic loop encompassing residues 309−321 adopts a helical conformation from 317 to 321 in the PXR−hyperforin structure, which we denote α6 (Figure 2B). This region of PXR is not impacted by crystal contacts and thus

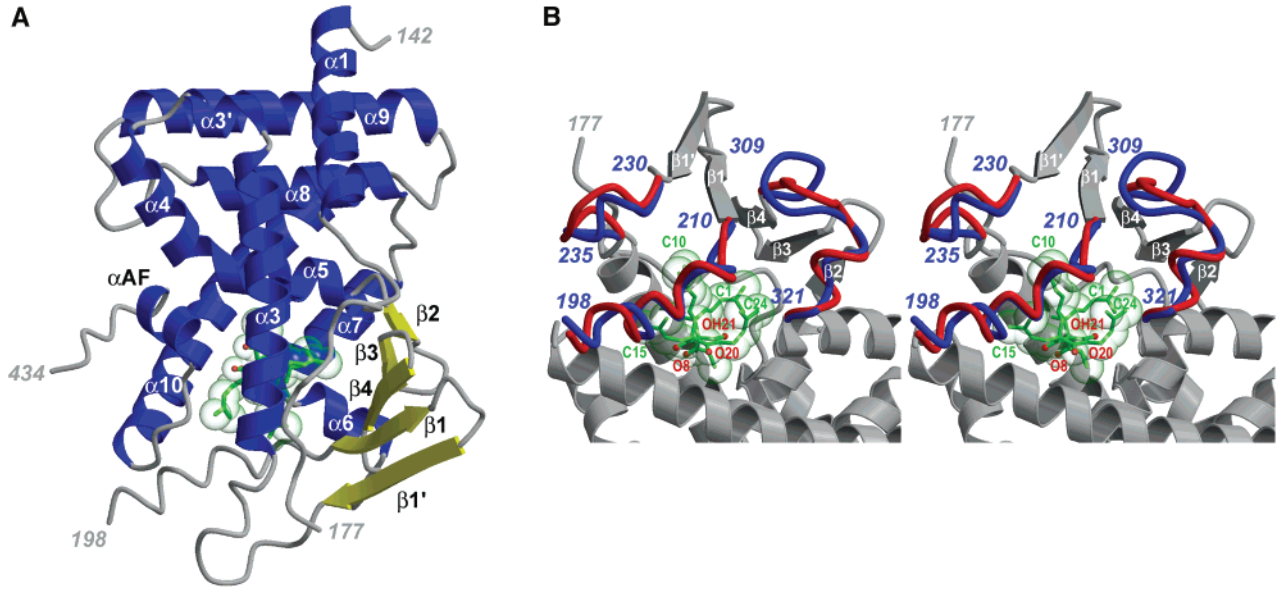

FIGURE 2: Crystal structure of human PXR in complex with hyperforin. (A) 2.1 Å crystal structure of the ligand binding domain of human PXR bound to hyperforin, an active component of St. John's wort. PXR residues 142−177 and 198−434 are shown with α helices in blue and β strands in yellow; hyperforin is rendered in green. The activation function 2 helix, which mediates interactions with transcriptional coactivators and corepressors, is also labeled (αAF). (B) Stereoview of a superposition between the PXR−hyperforin (red) and PXR−SR12813 (blue) (*15*) complexes. The α-helix 6 novel to the hPXR-LBD/hyperforin structure is labeled in red. Shifts in the loops between residues 198−210 and between residues 230−235 are also shown.

is free to adopt variant conformations in different PXR structures. This novel α6 in PXR is distinct from the α6's observed in other nuclear receptors (*34*−*44*) as it is perpendicular to α7. The α6's in other nuclear receptors occupy the same space as the 198−210 pseudo-helical region in PXR. Thus, the binding of hyperforin causes two loops adjacent to the ligand binding cavity to adopt unique conformations relative to PXR structures elucidated previously.

Binding of Hyperforin to PXR. The 2.5 Å dataset of PXR without ligand bound (*15*) allowed for the calculation of an unbiased 2.5 Å $|F_{obs}^{hyperforin}| - |F_{obs}^{apo}|$ electron density map. This density clearly showed the predicted chair orientation of the hyperforin ring structure as well as additional density indicating the positions of the more mobile aliphatic arms. Hyperforin was positioned as a single, full occupancy orientation into this density in the ligand binding pocket of PXR (Figure 3A). The $|F_{obs}| - |F_{obs}|$ density shown in Figure 3A does not cover regions of the hyperforin ligand, including portions of the C10 and C15 arms. However, as shown in Figure 3B, 2.5 Å $|F_{obs}^{apo}| - |F_{calc}^{apo}|$ difference density from the apo PXR structure (*15*) reveals positive peaks that help to explain why incomplete or disconnected density is observed in the $|F_{obs}^{hyperforin}| - |F_{obs}^{apo}|$ map used to place hyperforin. In addition, the presence of steric clashes, the loss of hydrogen bonds, and the movement of aliphatic arms out of electron density prohibits the placement of an alternate 180° rotation of the hyperforin chair into the PXR binding pocket.

The long aliphatic arms of hyperforin make several hydrophobic contacts with nonpolar amino acid side chains that line the ligand binding pocket (Figure 3C,D). For example, the C10 arm contacts Leu-209 and Met-243; the C15 arm contacts Leu-240, Ile-414, and Phe-420; and the C24 arm contacts Phe-281, Trp-299, and Met-323. The longer, six-carbon C1 arm contacts two aromatic residues, Phe-288 and Trp-299 (Figure 3C,D). The O8, O20, and OH21 oxygen atoms of hyperforin form short (2.5−2.7 Å) hydrogen bonds with the side chains of Ser-247, His-407, and Gln-285, respectively, within the ligand binding cavity. Two ordered water molecules are also observed within the pocket (Figure 3C).

Hyperforin, a 27 nM affinity ligand for human PXR, contacts a total of 12 amino acid side chains within the ligand binding pocket. Similar to previous PXR structures, hyperforin does not interact directly with residues in the AF-2 helix of the receptor. Hyperforin contacts one residue, Ile-414, not previously observed in PXR's interaction with the three orientations of SR12813, a 41 nM affinity ligand for PXR (*15*). In contrast, the three orientations of SR12813 contact five hydrophobic amino acid side chains: Leu-206, Met-246, Phe-251, Cys-284, and Leu-324, and one polar side chain, Ser-208, that hyperforin does not contact (*15*). These observations support the conclusion that there exists some level of plasticity in the manner in which PXR contacts ligands within the binding pocket.

Hyperforin Expands the PXR Ligand Binding Pocket. A comparison of the ligand binding cavities of the apo, SR12813 (*15*), and hyperforin structures reveals that PXR is able to change the shape of its binding pocket to conform to bound ligands (Figure 4). The binding cavity of apo-PXR is 1294 $Å^3$ in volume and includes solvent accessible (3.1 Å diameter) and solvent inaccessible (1.7 Å) pores to the surface of the molecule (Figure 4A). In addition, the side chain of His-407 swings out into the ligand binding pocket in the apo-PXR structure. In the SR12813−PXR complex, the binding pocket shrinks slightly to 1280 $Å^3$ and opens a solvent inaccessible pore (2.1 Å) distinct from the apo cavity (Figure 4B). In this complex, the side chain of His-407 has moved away from the interior of the pocket, and the side chain of Leu-209 closes over the solvent accessible channel observed in the apo structure. The shape of the binding

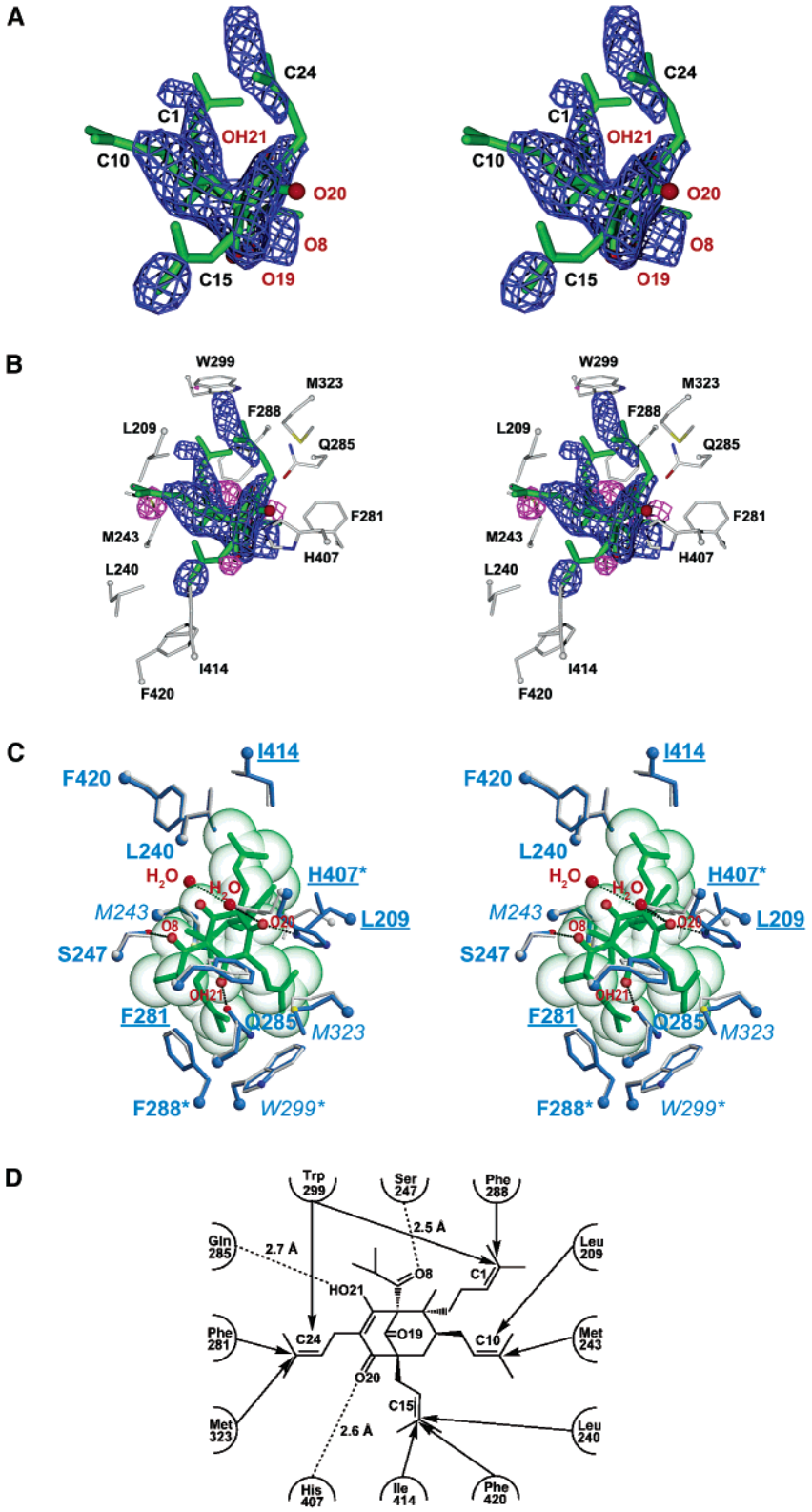

FIGURE 3: Interactions between hyperforin and human PXR. (A) Stereoview of unbiased 2.5 Å resolution $|F_{obs}^{hyperforin}| - |F_{obs}^{apo}|$ electron density for hyperforin in the binding cavity of PXR (contoured at 2.5σ). The four hyperforin oxygens are labeled, as well as the four aliphatic arms. (B) Stereoview of 2.5 Å resolution $|F_{obs}^{apo}| - |F_{calc}^{apo}|$ electron density (pink; contoured at 2.5σ), along with the same $|F_{obs}^{hyperforin}| - |F_{obs}^{apo}|$ density shown in panel A (blue; contoured at 2.5σ). The side chains that contact hyperforin (green) are also shown. (C) Stereoview of the contacts between hyperforin and PXR. Side chains that interact with hyperforin are rendered in blue; their equivalent positions in the apo-PXR structure (*15*) are rendered in white. The four hyperforin oxygens are indicated, including the single hydroxyl group and three carbonyl oxygens. Two water molecules present in the binding pocket are rendered in red. PXR forms several hydrogen bonds (dotted lines) with hyperforin: Ser-247 with carbonyl oxygen (2.5 Å); His-407 with a ring carbonyl (2.6 Å; also stabilized by a 3 Å hydrogen bond to water); and Gln-285 with the hyperforin hydroxyl group (2.7 Å). The four amino acid side chains shown in Figure 4 are underlined; the three side chains shown in Figure 5A are in italics; the three amino acids we examine by mutagenesis are indicated with asterisks. (D) Schematic representation of the contacts between hyperforin and the ligand binding pocket of human PXR. Nonpolar contacts are represented by solid lines, and hydrogen bonds are represented by dotted lines.

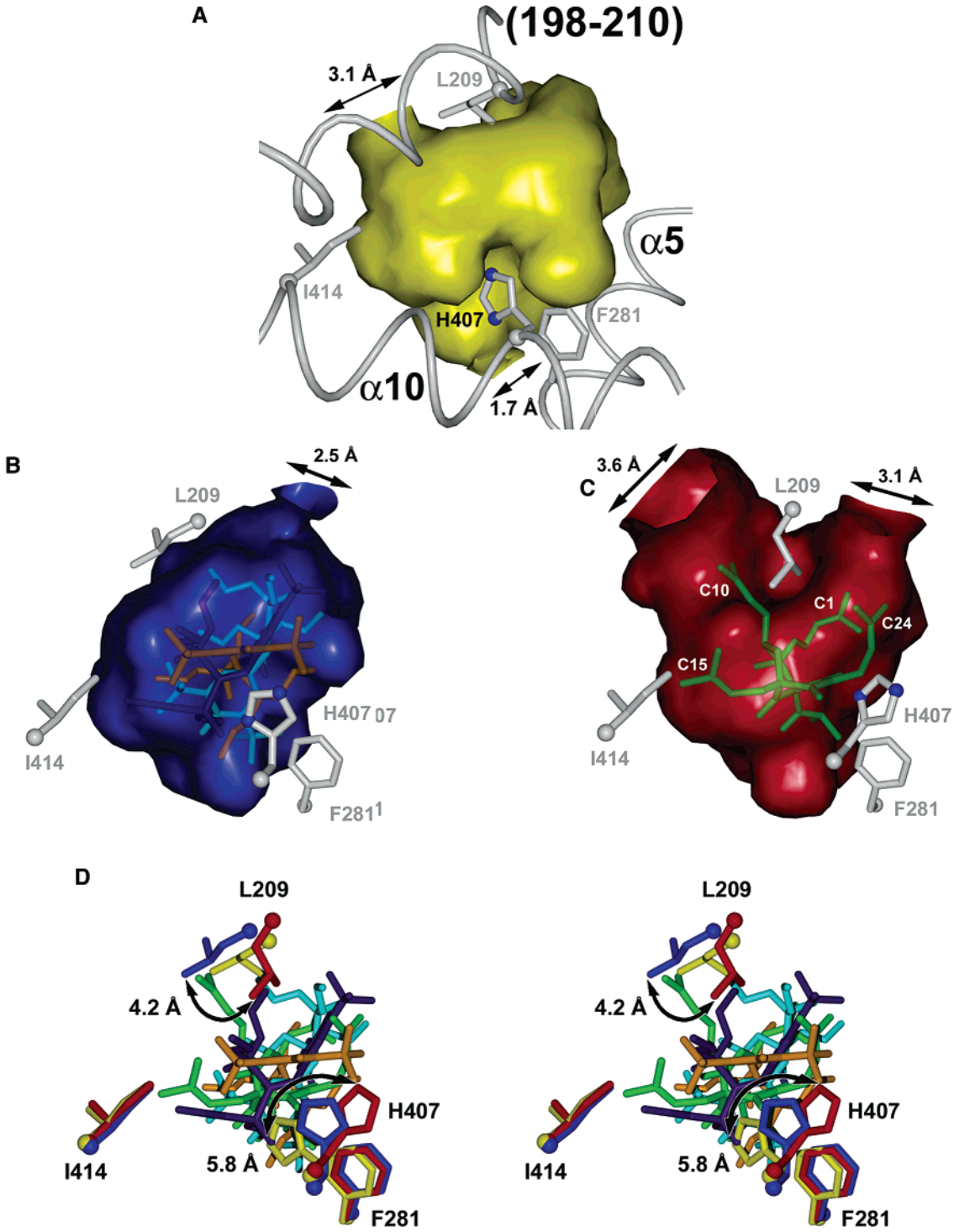

FIGURE 4: Hyperforin expands the ligand binding pocket of PXR**.** Panels A−D are in the same orientation, viewed roughly from above relative to Figure 3A, and each shows the positions of the following amino acid side chains: Leu-209, Phe-281, His-407, and Ile-414. (A) Molecular surface of the ligand binding cavity of apo-PXR (yellow) with an α carbon trace showing the mobile pseudohelical region (residues 198−210) and helices α5 and α10. (B) Molecular surface of the binding cavity of SR12813−PXR (blue) with the three bound orientations of SR12813 (cyan, indigo, and orange). (C) Molecular surface of the ligand binding cavity of hyperforin−PXR (red) with hyperforin bound (green). (D) Stereoview of the movement of two amino acid side chains adjacent to the PXR ligand binding pocket, Leu-209 and His-407, central to the conformability of the pocket to specific ligands.

pocket in the SR12813 complex is roughly elliptical. The binding cavity of the PXR−hyperforin complex, in contrast, changes in shape and expands significantly to 1544 Å^3 (Figure 4C). The side chain of His-407 has moved even further away from the interior of the pocket, but the side chain of Leu-209 is now positioned within the pocket between the C1 and C10 aliphatic arms of hyperforin. The presence of the hyperforin molecule and the movement of Leu-209 generates two solvent accessible pores in the PXR−hyperforin complex (Figure 4C).

The volume of the ligand binding pocket in the PXR−hyperforin complex approaches the largest pocket described for a nuclear receptor, that of PPARγ at 1619 Å^3 (*39*). The increase in the volume of the PXR ligand binding pocket is

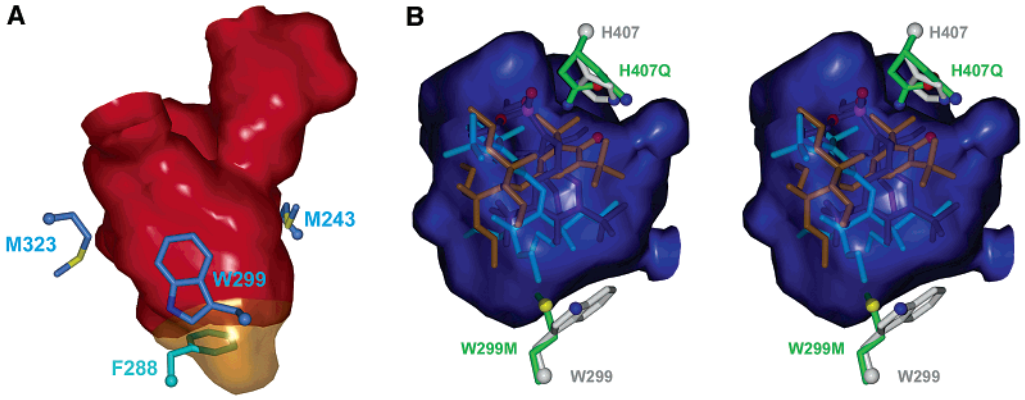

FIGURE 5: Modeling the impact of single-site mutations on the activation of PXR by specific ligands. Panels A−B are viewed in roughly the same orientation as Figure 3C. (A) Mutation of Phe-288 (cyan) to alanine expands the molecular surface of the PXR−hyperforin binding cavity (red) by the amount indicated (orange). (B) Stereoview showing that the mutation of Trp-299 to methionine increases the hydrophobic flexibility of the side chain adjacent to the three orientations of SR12813 (cyan, indigo, and orange), while mutation of His-407 to glutamine increases the polar flexibility adjacent to the polar atoms (oxygens in red) of positions 2 and 3 of SR12813.

generated largely by movement of two side chains and two regions of main chain (Figure 4D). Leu-209 shifts by 4.2 Å between the SR12813 and hyperforin complexes, and His-407 shifts by 5.8 Å between the apo and hyperforin structures. The main-chain moves by up to 1.6 and 3.3 Å in the mobile 207−210 and 230−235 regions, respectively, between the apo and the hyperforin structures. These structural changes work in concert to expand the ligand binding pocket by ~250 Å^3. Thus, the ligand binding cavity of PXR appears to employ an induced fit mechanism to accommodate different ligands. This remarkable binding pocket flexibility is likely to be an important determinant of the permissive ligand binding properties of PXR, enabling this promiscuous receptor to expand the chemical space it can sample.

Single-Site Mutants that Impact Ligand Activation. Targeted mutations of residues within the binding pocket of PXR have been shown to have dramatic effects on the ability of ligands to activate this receptor (*15*). Thus, despite its promiscuity, the activation of transcription by PXR appears to depend on interactions with specific residues within the pocket. We next sought to design mutants that altered the activation of the receptor by SR12813 and hyperforin in a predictable manner. In a previous study, we introduced mutations in the ligand binding pocket of PXR that impacted polar amino acid side chains (*15*). In this study, we chose to mutate aromatic side chains in the human PXR binding pocket. Accordingly, we introduced the following modest mutations of aromatic residues that contact both hyperforin and SR12813: Phe-288-Ala, Trp-299-Met, and His-407-Gln. Using the crystal structures of human PXR in complexes with SR12813 and hyperforin, we sought to predict the impact these mutations would have on the efficacy of these drugs. We hypothesized that the increased space introduced by the Phe-288-Ala mutation adjacent to the long, five-carbon C1 arm of hyperforin would improve the EC_{50} of this compound relative to SR12813 (Figure 5A). In contrast, the Trp-299-Met and His-407-Gln mutations were expected to improve the EC_{50} of SR12813 relative to hyperforin because of increased flexibility of hydrophobic and polar side chains, respectively, adjacent to SR12813 (Figure 5B).

Using reporter gene assays in transiently transfected CV-1 cells, we determined the response of these PXR variants to hyperforin, SR12813, and rifampicin (Table 3). Again, rifampicin was included because it is an established activator of human PXR (*3*, *4*). The EC_{50} values for the activation of wild-type PXR by hyperforin, SR12813, and rifampicin are 32.2, 127, and 463 nM, respectively. The Phe-288-Ala mutation exhibits improved activation by hyperforin (EC_{50} of 13.4 nM) and diminished activation by SR12813 (245 nM). In contrast, the Trp-299-Met and His-407-Gln mutants exhibit the opposite effect—each show improved activation by SR12813 (EC_{50} values of 78.0 and 76.8 nM, respectively) but diminished activation by hyperforin (80.4 and 56.7 nM, respectively). All three mutations decrease the EC_{50} of rifampicin to between ~750 and ~1100 nM. Rifampicin is 823 Da in mass as compared to 505 and 514 Da, respectively, for SR12813 and hyperforin. It has been previously hypothesized that rifampicin binds to PXR in a manner distinct from smaller ligands (*15*); thus, these mutations may have different effects on rifampicin binding than on SR12813 and hyperforin. In summary, the activation of PXR can be changed by altering the size of the ligand binding pocket or by introducing hydrophobic or polar flexibility in a rational manner.

DISCUSSION

St. John's wort is widely used in Europe and the United States to treat mild to moderate depression (*45*, *46*). There exists conflicting evidence, however, as to the true effectiveness of SJW in treating the symptoms of depression (*46*). In addition, a dangerous side effect of St. John's wort is its ability to accelerate the metabolism of prescription medicines including oral contraceptives, anti-HIV compounds, and immunosuppressants (*11*−*14*). These observations have raised concerns over the unregulated use of SJW by patients concurrently taking other clinical therapeutics.

The active agent in SJW is hyperforin, a 27 nM affinity ligand for human PXR (*8*, *47*−*50*) (Figure 1). We examined the regulation of drug metabolism gene expression in primary human hepatocytes treated with hyperforin. We found that hyperforin induces the expression of a variety of drug metabolism genes, including those encoding Phase I (oxidation) and Phase II (conjugation) enzymes, as well as Phase III (excretion) efflux pumps (Table 1). The gene activation profile exhibited by hyperforin treatment was similar to that

exhibited by rifampicin, another established PXR activator (*3*, *4*). The genes activated by hyperforin include those encoding for P450 enzymes (*7*, *51*), drug conjugating enzymes such as glutathione S-transferases, and drug efflux transporters such as MDR1 (*1*). The activation of these drug metabolism genes by hyperforin explains the dangerous drug−drug interactions caused by the co-administration of St. John's wort with other clinical therapeutics (*9*−*14*).

The 2.1 Å crystal structure of human PXR in complex with hyperforin reveals that the PXR ligand binding domain uses an induced fit mechanism to accommodate structurally distinct ligands (Figure 2A, Table 2). Hyperforin contacts nine hydrophobic and three polar amino acid side chains that line the ligand binding cavity of human PXR (Figure 3C,D). In the previous structure of PXR in complex with the cholesterol-lowering compound SR12813, this ligand was observed bound in three distinct orientations within the PXR binding pocket (*15*). In that structure, however, the maximum number of hydrophobic residues contacted by SR12813 was seven (position 2), the maximum number of polar contacts was three (position 3), and no orientation contacted more than nine PXR residues. Thus, hyperforin makes more nonpolar and polar interactions than SR12813 did, helping to explain its high affinity binding to PXR.

Hyperforin was also found to expand the ligand binding pocket by up to 250 $Å^3$ and to open two large, solvent accessible channels to the surface of the molecule (Figure 3). PXR appears to use mobile main chain and side chain regions to change its ligand binding pocket to accommodate different ligands. For example, the main chain region of residues 207−210 moves by 1.6 Å, and the side chains Leu-209 and His-407 move by 4.2 and 5.8 Å, respectively, relative to PXR structures determined previously (*15*). Thus, PXR is able to breath by expanding and contacting as ligands of different sizes and shapes bind to the receptor. This observation advances our understanding of how PXR detects drugs and other xenobiotics of diverse shapes and sizes (*4*, *6*, *52*). Whereas PXR's ligand binding pocket was previously thought to be relatively rigid and to use a neutral shape to accommodate different ligands (*15*), it is now clear that the pocket can conform to specific compounds and appears to use an induced fit mechanism (*53*). Indeed, expansion is likely to be necessary for PXR to bind to the macrocyclic antibiotic rifampicin (823 Da vs 514 and 505 Da for hyperforin and SR12813, respectively), which is too large to fit in any of the currently resolved PXR binding pockets.

Mutations within the ligand binding cavity of PXR are known to impact the ability for the receptor to respond to distinct ligands (*15*). In the past, we have examined the role of polar residues in PXR's response to ligands by mutating residues that differ between mouse and human PXR (*15*). In this work, we chose to examine the impact of mutating aromatic residues that line the PXR ligand binding pocket. Six of the 20 amino acid side chains that line the binding cavity of human PXR are aromatic. By using the structures of SR12813- and hyperforin-bound PXR to guide our choice of mutations, we were able to alter the relative effectiveness of ligands for PXR (Figure 5). Two single-site mutations, Trp-299-Met and His-407-Gln, generate forms of PXR that are more responsive to SR12813 and less responsive to hyperforin relative to wild-type PXR (Table 3). In contrast, a Phe-288-Ala mutant is more responsive to hyperforin and less responsive to SR12813. These results indicate that small changes within the PXR binding pocket can have large effects on the ligand-dependent activation of this receptor. These results also suggest that rational protein design may be useful in altering the ligand specificity of PXR.

The PXR−hyperforin crystal structure should enable the generation of novel hyperforin analogues that do not activate PXR. Such compounds may be useful for treating mild depression. However, the structure presented here indicates that the development of a detailed, structure-based pharmacophore for PXR to predict and eliminate drug−drug interactions (*33*, *54*, *55*) may be more difficult than originally appreciated. Given the ability of the PXR ligand binding cavity to expand and contract depending on the character of the bound ligand, our ability to extrapolate a series of rules for PXR's binding determinants based on a small number of crystal structures will be difficult. At this point, the determination of more crystal structures of PXR bound to structurally distinct ligands appears to be the most effective way to elucidate how PXR detects and protects the body from harmful chemicals.

ACKNOWLEDGMENT

The authors wish to thank members of the Redinbo laboratory, Charlie Carter (UNC Chapel Hill), and Tim Willson (GlaxoSmithKline) for support and stimulating discussions.

REFERENCES

1. Goodwin, B., Redinbo, M. R., and Kliewer, S. A. (2002) *Annual Review of Pharmacology & Toxicology 42*, 1−23.
2. Xie, W., and Evans, R. M. (2001) *Journal of Biological Chemistry 276*, 37739−42.
3. Lehmann, J. M., McKee, D. D., Watson, M. A., Willson, T. M., Moore, J. T., and Kliewer, S. A. (1998) *J. Clin. Invest. 102*, 1016−23.
4. Blumberg, B., Sabbagh, W., Jr., Juguilon, H., Bolado, J., Jr., van Meter, C. M., Ong, E. S., and Evans, R. M. (1998) *Genes Dev. 12*, 3195−205.
5. Schuetz, E. G., Brimer, C., and Schuetz, J. D. (1998) *Mol. Pharmacol. 54*, 1113−7.
6. Synold, T. W., Dussault, I., and Forman, B. M. (2001) *Nat. Med. 7*, 584−90.
7. Wentworth, J. M., Agostini, M., Love, J., Schwabe, J. W., and Chatterjee, V. K. (2000) *J. Endocrinol. 166*, R11−6.
8. Moore, L. B., Goodwin, B., Jones, S. A., Wisely, G. B., Serabjit-Singh, C. J., Willson, T. M., Collins, J. L., and Kliewer, S. A. (2000) *Proc. Natl. Acad. Sci. U.S.A. 97*, 7500−2.
9. Mathijssen, R. H., Verweij, J., de Bruijn, P., Loos, W. J., and Sparreboom, A. (2002) *J. Natl. Cancer Inst. 94*, 1247−9.
10. Ernst, E., Rand, J. I., Barnes, J., and Stevinson, C. (1998) *Eur. J. Clin. Pharmacol. 54*, 589−94.
11. Ernst, E. (1999) *Lancet 354*, 2014−6.
12. Fugh-Berman, A. (2000) *Lancet 355*, 134−8.
13. Piscitelli, S. C., Burstein, A. H., Chaitt, D., Alfaro, R. M., and Falloon, J. (2000) *Lancet 355*, 547−8.
14. Ruschitzka, F., Meier, P. J., Turina, M., Luscher, T. F., and Noll, G. (2000) *Lancet 355*, 548−9.
15. Watkins, R. E., Wisely, G. B., Moore, L. B., Collins, J. L., Lambert, M. H., Williams, S. P., Willson, T. M., Kliewer, S. A., and Redinbo, M. R. (2001) *Science 292*, 2329−33.
16. Otwinowski, Z., Minor, W. (1993) *Data collection and processing*, Warrington, UK.
17. Navaza, J., and Saludjian, P. (1997) *Methods Enzymol. 276A*, 581−94.
18. Jones, T. A., Zou, J. Y., Cowan, S. W., and Kjeldgaard, M. (1991) *Acta Crystallogr. A 47*, 110−19.
19. Brunger, A. T., Adams, P. D., Clore, G. M., DeLano, W. L., Gros, P., Grosse-Kunstleve, R. W., Jiang, J. S., Kuszewski, J., Nilges,

M., Pannu, N. S., Read, R. J., Rice, L. M., Simonson, T., and Warren, G. L. (1998) *Acta Crystallogr. D 54*, 905−21.
20. Nicholls, A., Sharp, K., and Honig, B. (1991) *Proteins: Struct., Funct., Genet. 11*, 281.
21. Kraulis, P. J. (1991) *J. Appl. Crystallogr. 24*, 946−50.
22. *DINO: Visualizing Structural Biology*, (2001), http://www.dino3d.org.
23. Goodwin, B., Hodgson, E., and Liddle, C. (1999) *Mol. Pharmacol. 56*, 1329−39.
24. Hennessy, M., Kelleher, D., Spiers, J. P., Barry, M., Kavanagh, P., Back, D., Mulcahy, F., and Feely, J. (2002) *Br. J. Clin. Pharmacol. 53*, 75−82.
25. Wang, Z., Gorski, J. C., Hamman, M. A., Huang, S. M., Lesko, L. J., and Hall, S. D. (2001) *Clin. Pharmacol. Ther. 70*, 317−26.
26. Bray, B. J., Perry, N. B., Menkes, D. B., and Rosengren, R. J. (2002) *Toxicol. Sci. 66*, 27−33.
27. Maglich, J. M., Stoltz, C. M., Goodwin, B., Hawkins-Brown, D., Moore, J. T., and Kliewer, S. A. (2002) *Mol. Pharmacol. 62*, 638−46.
28. Geick, A., Eichelbaum, M., and Burk, O. (2001) *J. Biol. Chem. 276*, 14581−7.
29. Savas, U., Griffin, K. J., and Johnson, E. F. (1999) *Mol. Pharmacol. 56*, 851−7.
30. Lewis, D. F. V., Eddershaw, P. J., Dickins, M., Tarbit, M. H., and Goldfarb, P. S. (1998) *Chem.-Biol. Interact. 115*, 175−199.
31. Nadin, L., and Murray, M. (1999) *Biochem. Pharmacol. 58*, 1201−8.
32. Miners, J. O., and Birkett, D. J. (1998) *Br. J. Clin. Pharmacol. 45*, 525−38.
33. Watkins, R. E., Noble, S. M., and Redinbo, M. R. (2002) *Curr. Opin. Drug Discov. Devel. 5*, 150−8.
34. Matias, P. M., Donner, P., Coelho, R., Thomaz, M., Peixoto, C., Macedo, S., Otto, N., Joschko, S., Scholz, P., Wegg, A., Basler, S., Schafer, M., Egner, U., and Carrondo, M. A. (2000) *J. Biol. Chem. 275*, 26164−71.
35. Egea, P. F., Mitschler, A., Rochel, N., Ruff, M., Chambon, P., and Moras, D. (2000) *EMBO J. 19*, 2592−601.
36. Rochel, N., Wurtz, J. M., Mitschler, A., Klaholz, B., and Moras, D. (2000) *Mol. Cell 5*, 173−9.
37. Xu, H. E., Lambert, M. H., Montana, V. G., Parks, D. J., Blanchard, S. G., Brown, P. J., Sternbach, D. D., Lehmann, J. M., Wisely, G. B., Willson, T. M., Kliewer, S. A., and Milburn, M. V. (1999) *Mol. Cell 3*, 397−403.
38. Oberfield, J. L., Collins, J. L., Holmes, C. P., Goreham, D. M., Cooper, J. P., Cobb, J. E., Lenhard, J. M., Hull-Ryde, E. A., Mohr, C. P., Blanchard, S. G., Parks, D. J., Moore, L. B., Lehmann, J. M., Plunket, K., Miller, A. B., Milburn, M. V., Kliewer, S. A., and Willson, T. M. (1999) *Proc. Natl. Acad. Sci. U.S.A. 96*, 6102−6.
39. Nolte, R. T., Wisely, G. B., Westin, S., Cobb, J. E., Lambert, M. H., Kurokawa, R., Rosenfeld, M. G., Willson, T. M., Glass, C. K., and Milburn, M. V. (1998) *Nature 395*, 137−43.
40. Brzozowski, A. M., Pike, A. C. W., Dauter, Z., Hubbard, R. E., Bonn, T., Engstrom, O., Ohman, L., Greene, G. L., Gustafsson, J.-A., and Carlquist, M. (1997) *Nature 389*, 753−8.
41. Wagner, R. L., Apriletti, J. W., McGrath, M. E., West, B. L., Baxter, J. D., and Fletterick, R. J. (1995) *Nature 378*, 690−7.
42. Renaud, J.-P., Rochel, N., Ruff, M., Vivat, V., Chambon, P., and Moras, D. (1995) *Nature 378*, 681−9.
43. Williams, S. P., and Sigler, P. B. (1998) *Nature 393*, 392−6.
44. Bourguet, W., Ruff, M., Chambon, P., Gronemeyer, H., and Moras, D. (1995) *Nature 375*, 377−82.
45. Deltito, J., and Beyer, D. (1998) *J. Affect Disord. 51*, 345−51.
46. Shelton, R. C., Keller, M. B., Gelenberg, A., Dunner, D. L., Hirschfeld, R., Thase, M. E., Russell, J., Lydiard, R. B., Crits-Cristoph, P., Gallop, R., Todd, L., Hellerstein, D., Goodnick, P., Keitner, G., Stahl, S. M., and Halbreich, U. (2001) *JAMA 285*, 1978−86.
47. Muller, W. E., Singer, A., Wonnemann, M., Hafner, U., Rolli, M., and Schafer, C. (1998) *Pharmacopsychiatry 31 Suppl. 1*, 16−21.
48. Laakmann, G., Schule, C., Baghai, T., and Kieser, M. (1998) *Pharmacopsychiatry 31 Suppl. 1*, 54−9.
49. Chatterjee, S. S., Bhattacharya, S. K., Wonnemann, M., Singer, A., and Muller, W. E. (1998) *Life Sci. 63*, 499−510.
50. Kaehler, S. T., Sinner, C., Chatterjee, S. S., and Philippu, A. (1999) *Neurosci. Lett. 262*, 199−202.
51. Moore, J. T., and Kliewer, S. A. (2000) *Toxicology 153*, 1−10.
52. Jones, S. A., Moore, L. B., Shenk, J. L., Wisely, G. B., Hamilton, G. A., McKee, D. D., Tomkinson, N. C., LeCluyse, E. L., Lambert, M. H., Willson, T. M., Kliewer, S. A., and Moore, J. T. (2000) *Mol. Endocrinol. 14*, 27−39.
53. Hammes, G. G. (2002) *Biochemistry 41*, 8221−8.
54. Ekins, S., de Groot, M. J., and Jones, J. P. (2001) *Drug Metab. Dispos. 29*, 936−44.
55. Berretty, R.-P., Hsu, D., Kettner, L., Mascarenhas, A., Redinbo, M. R., Snoeyink, J., and Watkins, R. E. (2002) Ligand binding to the pregnane X receptor by geometric matching of hydrogen bonds, in *Currents in Computational Molecular Biology (RECOMB)* (Florea, L., Walenz, B., and Hannenhalli, S., Eds.) pp 22−23.

BI0268753